INTERNATIONAL JOURNAL OF CLIMATOLOGY
Int. J. Climatol. (2010)
Published online in Wiley InterScience
(www.interscience.wiley.com) DOI: 10.1002/joc.2119

RMetS
Royal Meteorological Society

High-resolution modelling of the potential impact of land surface conditions on regional climate over Indochina associated with the diurnal precipitation cycle

Hiroshi G. Takahashi,[a]*†‡ Takao Yoshikane,[a] Masayuki Hara,[a] Kumiko Takata[a] and Tetsuzo Yasunari[a,b]

[a] *Frontier Research Center for Global Change (FRCGC), Japan Agency for Marine-Earth Science and Technology (JAMSTEC), Yokohama, Japan*

[b] *Hydrospheric Atmospheric Research Center (HyARC), Nagoya University, Nagoya, Japan*

ABSTRACT: This study examined the impact of changes in land surface conditions on regional climate over Indochina using a high-resolution regional climate model. Anthropogenically induced land surface changes are going on in this part of tropical Southeast Asia. Because a previous study suggested that deforestation in this area affected September precipitation, we chose September as the study period. We performed a control simulation (CTL) driven by reanalysis data combined with current land use and predicted soil moisture data. The CTL reproduced the spatial distribution of total precipitation well. In addition, it also simulated a distinct diurnal cycle of precipitation that was previously reported in observational studies. Two sensitivity experiments, assuming wetter and drier land surface conditions over the Khorat Plateau (northeast Thailand) compared with the current land surface condition, were conducted and examined the impact of land surface changes on precipitation. The results indicated that drier land surface conditions increased precipitation over the disturbed region. A pronounced increase in precipitation was found only during nighttime, which coincided with the peak in the climatological diurnal precipitation cycle. Climatologically, the diurnal peak in precipitation occurs from evening to early morning over the Khorat Plateau. Drier conditions intensified the diurnal variation of precipitable water associated with the thermally induced local circulation responsible for a horizontal gradient of near-surface temperature. The effects of land use and land cover changes in the tropics are shown to be strongly related to the diurnal precipitation cycle. Copyright © 2010 Royal Meteorological Society

KEY WORDS land surface condition; Southeast Asian monsoon; diurnal cycle in precipitation; thermally induced local circulation; precipitable water; regional climate change; regional climate modelling

Received 28 November 2008; Revised 11 December 2009; Accepted 5 January 2010

1. Introduction

Land use and land cover changes (LUCCs) may impact regional climates as well as the global climate. In the tropics, one of the largest LUCCs is deforestation. The Asian monsoon region, including the Indochina Peninsula and the maritime continent, has experienced intensive anthropogenic deforestation since the latter half of the 20th century (e.g. Ramankutty and Foley, 1999).

Over the past three decades, various global climate modelling studies have examined the potential impacts of deforestation on regional and global climates (e.g. Henderson-Sellers and Gornitz, 1984; Dickinson and Henderson-Sellers, 1988; Lean and Warrilow, 1989; Shukla *et al*., 1990). Using coarse-resolution global and regional climate models (GCM and RCM, respectively), some studies have conducted experiments with recorded LUCC data to examine the effects of historical LUCCs on global climate (e.g. Chase *et al*., 2000; Kanae *et al*., 2001; Brovkin *et al*., 2006). Although these modelling studies have provided somewhat different results, they have generally agreed that deforestation leads to reduced precipitation and evaporation and increased surface temperature in the disturbed regions.

Pielke (2001) argued that land surface changes affect both regional and global climates. He noted that some studies have shown a decrease in precipitation due to deforestation or conversion from original vegetation to cultivation, whereas others have found an increase in precipitation. A decrease in precipitation would likely relate to a decrease in water vapour from the surface or in convective available potential energy (Pielke, 2001). Studies showing that LUCCs can enhance convection and increase precipitation have implicated thermally induced local circulation due to horizontally inhomogeneous sensible heating created by different surface properties (e.g.

* Correspondence to: Hiroshi G. Takahashi, 3173-25 Showamachi, Kanazawa-ku, Yokohama, Kanagawa 236-0001, Japan.
E-mail: hiroshi3@jamstec.go.jp
† Current address: Research Institute for Global Change, Japan Agency for Marine-Earth Science and Technology, Yokohama, Japan.
‡ Current address: Graduate School of Urban Environmental Science, Tokyo Metropolitan University, Tokyo, Japan.

Ookouchi *et al*., 1984; Segal and Arritt, 1992; Emori, 1998).

D'Almeida *et al*. (2007) discussed observational and mesoscale modelling studies of the impacts of LUCCs on precipitation and convective activity over the Amazon. They noted that few observational and mesoscale modelling studies have shown reduced precipitation or suppressed convective activity under deforested conditions. The results of observations and mesoscale modelling are inconsistent with the reduced precipitation predicted by GCMs and coarse-resolution RCMs (D'Almeida *et al*., 2007). Consequently, D'Almeida *et al*. (2007) concluded that, from local to regional scales, LUCC intensifies convective activity by creating horizontally inhomogeneous near-surface temperature. Recently, a possible impact of LUCCs on regional climate was examined over the South Asian monsoon region using satellite-derived normalized difference vegetation index (NDVI) and precipitation datasets. The result suggested that a decrease in the thermal contrast between land and sea due to intensive irrigation over land might induce a decrease in precipitation in that region (Lee *et al*., 2009). This observational finding may be explained by the mechanism discussed by D'Almeida *et al*. (2007).

Most studies on the impacts of deforestation have used GCMs or coarse-resolution RCMs. However, models with horizontal resolutions coarser than approximately 50 km cannot resolve regional-scale terrain and land use. For this reason, it is quite difficult to capture regional climate. More examinations of the climatological effects of regional-scale LUCCs on regional climates using high-resolution models are needed. In particular, no previous high-resolution studies have examined the climatological effects of regional-scale LUCCs on the regional climate over the Asian monsoon region although this area has experienced intensive LUCCs. In this study, we focused on the Indochina Peninsula, where deforestation has occurred in northeast Thailand over the last century. In addition, Kanae *et al*. (2001) found a decreasing trend of observed precipitation in September over the Indochina Peninsula. They used a coarse-resolution RCM and suggested that the decreasing trend may be associated with a decrease in evapotranspiration due to the recorded deforestation. However, as mentioned above, their coarse-resolution RCM could not reproduce local circulations due to regional-scale terrain and horizontally inhomogeneous sensible heating created by different surface properties. Therefore, it is necessary to examine the impact of LUCCs using a high-resolution model. To discuss the observed decrease in September precipitation, we chose September as our study period.

Another major issue in the use of models with coarse horizontal resolution is the need for cumulus convective parameterization (CCP) to involve subgrid-scale convective activity. However, there are many uncertainties associated with CCP, and these parameterizations have different sensitivities to dynamic and thermodynamic fields, as shown even when using an approximately 30-km mesoscale model (Pan *et al*., 1996). Furthermore, CCP cannot reproduce the observed diurnal cycle of precipitation (e.g. Dai and Trenberth, 2004; Dai, 2006). Precipitation in the tropics, in particular, is characterized as convective precipitation. Recent studies using tropical rainfall measurement mission precipitation radar (TRMM-PR) data have described distinct diurnal variations in precipitation (e.g. Hirose and Nakamura, 2005). Even when the horizontal resolution of several atmospheric general circulation models (AGCMs) were improved to 0.5°, the diurnal cycle in precipitation still deviated from observations, probably due to the CCP (Lee *et al*., 2007). Hara *et al*. (2009) demonstrated that for an AGCM with a 20-km grid, the CCP produced significant error in the diurnal cycle and spatial distribution of precipitation over the maritime continent. Thus, the reproduced climates and possible impacts of LUCCs over the tropics strongly depend on the characteristics of CCP because the CCP produces most of the precipitation. To examine impacts of regional-scale LUCCs over tropical regions, numerical models should be able to reproduce realistic regional climate, including the diurnal variation of precipitation.

Therefore, in this study we investigated the potential impact of intensive LUCCs over the Indochina Peninsula using a high-resolution RCM without CCP. Because tropical precipitation systems are generally nonlinear, we reduced the uncertainty by using a long-term (one-month period) simulation. Section 2 documents the experimental design. Section 3 presents results of the numerical experiments. Possible mechanisms behind the effects of LUCCs are discussed in Section 4, and conclusions are given in Section 5.

2. Experimental design

We used a convective system resolving model to simulate a realistic distribution of precipitation and local circulations related to terrain and land use. The advanced weather research and forecasting (WRF) modelling system (Skamarock *et al*., 2005), which is a nonhydrostatic RCM developed by the National Center for Atmospheric Research (NCAR), was chosen for this purpose. The 40-year reanalysis (ERA-40, Uppala *et al*., 2005) dataset of the European Centre for Medium-Range Weather Forecasts (ECMWF) and the extended reconstructed sea surface temperature (SST) V2 (Smith and Reynolds, 2004) datasets of the National Oceanic and Atmospheric Administration (NOAA) were used as initial and boundary conditions. Soil moisture and temperature data from ERA-40 were also used. The horizontal grid increment of the coarse domain was 25 km and that of the two-way nested domain was 5 km. The domains and terrain are shown in Figure 1(a). Both domains had 27 terrain-following vertical levels. Because preliminary experiments with CCP showed a very unrealistic precipitation distribution and diurnal pattern, we did not apply CCP in either domain. The WRF single-moment six-class microphysics scheme (Hong and Lim, 2006) and the Noah land

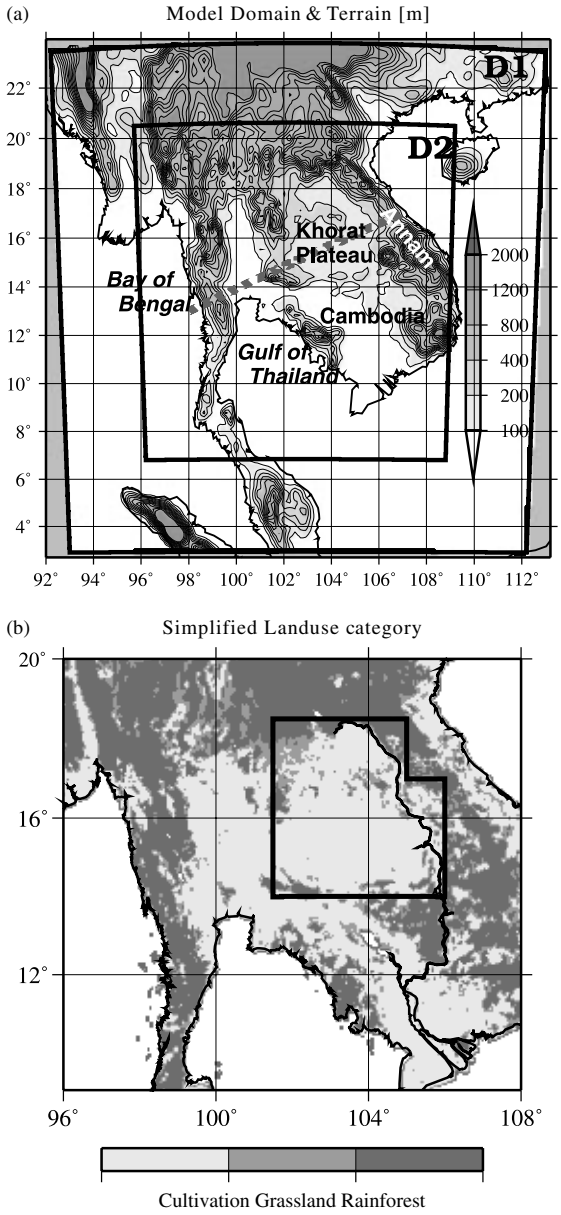

Figure 1. The upper panel (a) shows the terrain in the WRF model, and the lower panel (b) presents the land use categories. D1 (D2) in (a) indicates the coarse (nested) domain. Grey-dashed line in (a) is cross-section of Figure 12. The thick line in (b) indicates the assumed area of dense tropical rainforest (disturbed region).

surface model (Noah-LSM; Chen and Dudhia, 2001; Ek *et al*., 2003) were also used.

The Noah-LSM had one canopy layer and four soil layers down to 2 m, with the root zone in the upper 1 m. The surface skin temperature was determined by a surface energy balance equation for the combined ground–vegetation surface. The total evapotranspiration was the sum of the direct evaporation (E_{dir}) from the top soil layer, evaporation of precipitation intercepted by the canopy (E_{c}), and transpiration (E_{t}) by the canopy. E_{dir} and E_{c} were calculated by a Penman-based energy balance approach that included a stability-dependent aerodynamic resistance. The canopy resistance was calculated with empirical equations (Jacquemin and Noilhan, 1990).

The simulation with current land use (CTL) was performed three times from 30 August to 1 October in each year from 1998 to 2000. The first two days of the simulation (30 and 31 August) were assumed to be the spin up. We analysed one-month results from 1 to 30 September. The current land use was taken from 1992 data obtained from the United States Geological Survey (USGS). In the past, northeast Thailand was highly forested; however, the 1992 data categorized the majority of northeast Thailand as under cultivation. In the WRF model, the prime cultivated land use was given as 'irrigated cropland and pasture', and the tropical rainforest was described as 'evergreen broadleaf forest'. Figure 1(b) shows the spatial distribution of land use.

We also conducted two sensitivity experiments assuming dense rainforest with wet soil moisture (WET) and sparse forest with dry soil moisture (DRY) to understand the impact of changes in land surface conditions. The design of WET was based on that of Kanae *et al*. (2001). The CTL and WET experiments differed in regard to the surface condition over northeast Thailand. The inner area enclosed with the black thick line in Figure 1 was defined as the assumed area of dense tropical rainforest. For the WET experiment, all land uses of the disturbed region were given as evergreen broadleaf forest except for the water body category. The parameter of the green fraction was set to 90%, which is comparable with the fraction found in undisturbed areas of the Indochina Peninsula. Because the green fraction parameter indicates the green vegetation coverage in a model grid, dense (little deforested) and sparse (intensively deforested) rainforests were characterized by the difference of green fraction. Over the disturbed region, volumetric soil water content was forced to remain at 0.45 m^3/m^3 throughout the time integration. The value of volumetric soil water content was almost the same as that simulated just after a precipitation event.

To understand the extreme impacts of intensive deforestation, DRY experiments were also conducted. The surface condition was assumed to be dry, sparse forest. The spatial distribution of this land use category was the same as that for WET, but the green fraction was set to 20%, and volumetric soil water content was forced to remain at 0.20 m^3/m^3. This value for the green fraction can be found in intensively disturbed areas of the Indochina Peninsula. The volumetric soil water content was almost the same as that found in the dry season. The WET and DRY experiments were also conducted during September for three years from 1998 to 2000. These three years had less precipitation than other years of the second half of the 20th century according to the time series shown in Figure 5 from Takahashi and Yasunari (2008); a similar result was also obtained from an examination of area mean precipitation using Climate Prediction Center (CPC) merged analysis of precipitation (CMAP; Xie and Arkin, 1997) data for the Indochina Peninsula.

We used the TRMM-PR 2A25 precipitation product (Iguchi *et al*., 2000) included in the TRMM 3G68 version 6 product for evaluation of model reproducibility of

precipitation amount and the diurnal cycle of precipitation. Hereafter, these precipitation data are referred to simply as TRMM-PR. We analysed only precipitation observed by the PR. Because the study area was limited to the Indochina Peninsula, we used the unified local time along 105 °E. These data had a 0.5 × 0.5 grid resolution. We used eight years of TRMM-PR observations from 1998 to 2005. Hirose *et al*. (2008) investigated the issue of the sample number of TRMM-PR observations. They suggested that a minimum eight-year mean was likely needed to describe 3-hourly diurnal variations of precipitation because of the sparse observations of TRMM.

To evaluate the simulated atmospheric structure, we used 6-hourly soundings measured at Ubon Ratchathani (104.87 °E, 15.25 °N), Thailand, under the framework of the Global Energy and Water Cycle Experiment (GEWEX)-Asian Monsoon Experiment-Tropics (GAME-T).

The name of the Khorat Plateau, the key region of this study, sometimes causes misunderstanding. Although the Khorat Plateau is higher than the low-altitude plain around Bangkok, it is bordered by mountain ranges on its eastern, northern and western sides. Thus, the Khorat Plateau is basically a basin-shaped valley rather than a plateau. The region of the Khorat Plateau is almost coincident with the disturbed region (Figure 1).

3. Results

3.1. Performance of CTL

Before analysing the sensitivity experiments, we compared the precipitation simulated by CTL with the observed precipitation (Figure 2). Abundant precipitation was observed along the coasts of the eastern Bay of Bengal and eastern Gulf of Thailand, as well as the eastern coast of northern Vietnam (Figure 2). The peaks of the simulated precipitation were closely correlated with the peaks indicated by TRMM-PR. To further examine these spatial similarities, a spatial correlation coefficient r_s was calculated by the following equation:

$$r_s = \sum_{i=1}^{N}(x_i - \overline{x})(y_i - \overline{y}) \Big/ \sqrt{\sum_{i=1}^{N}(x_i - \overline{x})^2} \sqrt{\sum_{i=1}^{N}(y_i - \overline{y})^2} \quad (1)$$

where N is the number of grids, x_i is the eight-year average of total rainfall measured by TRMM-PR for September at the ith grid, y_i is the three-year average of simulated total precipitation for September at the ith grid, $\overline{x}$ is the average of all x_i, and $\overline{y}$ is the average of all y_i. The spatial resolution of simulated precipitation was converted to the spatial resolution of the observations. A value of 0.55 was calculated for r_s, which was statistically significant at the 99.9% confidence level, indicating that the monthly mean precipitation was well simulated. In addition, Takahashi *et al*. (2009) performed a long-term simulation for September with the same model parameter settings; that study showed that long-term (30-year) experiments can capture not only the spatial pattern of precipitation but also the total amount of precipitation, compared with rain gauge observations. They suggested that the precipitation amount indicated by TRMM-PR was relatively less than rain gauge observations. At the least, the spatial distribution of three-year precipitation of CTL was similar to the observed precipitation of the Indochina Peninsula.

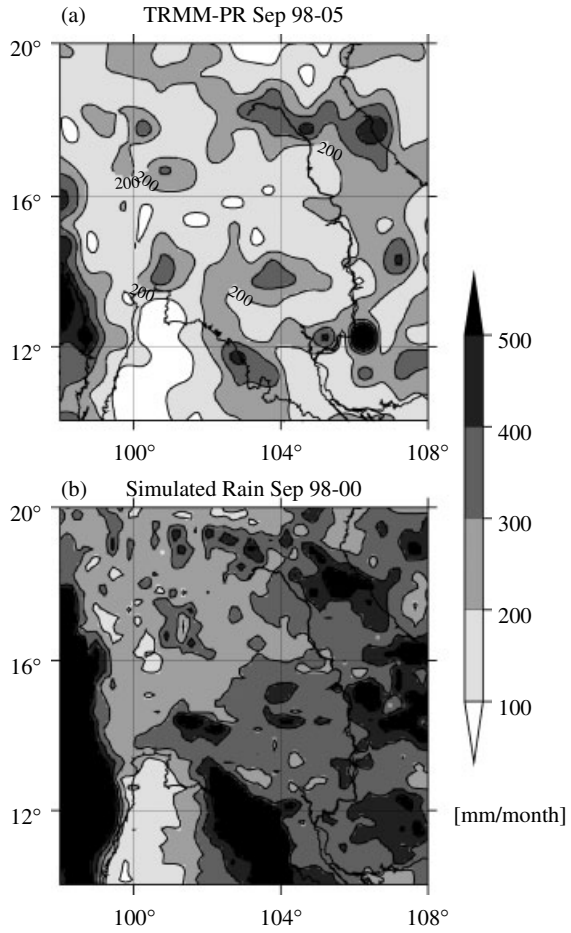

Figure 2. Total amounts of September precipitation over the Indochina Peninsula. (a) September precipitation averaged over eight years from 1998 to 2005 for September, observed by TRMM-PR. (b) The three-year averaged simulated precipitation.

Table I. Temporal correlation coefficient of daily mean zonal wind at 850 hPa (u850) and daily mean specific humidity at 925 hPa (sh925) between simulation (CTL) and observation (reanalysis).

Year	u850 (WRF JRA)	u850 (ERA JRA)	sh925 (WRF JRA)	sh925 (ERA JRA)
1998	0.93	0.98	0.59	0.71
1999	0.95	0.99	0.62	0.75
2000	0.98	0.99	0.67	0.89

The second and fourth column showed the correlation between two kinds of reanalysis datasets.
All values were statistically significant at the 99.9% confidence limit.

We also examined day-to-day variations of low-level zonal wind and specific humidity averaged over the 100°–104 °E, 12°–15°N region. Table I shows the temporal correlation coefficient for zonal wind and specific humidity between the simulations and observations (given by reanalysis data). Low-level zonal wind, namely the monsoon westerly, was well correlated with the observation data. Low-level humidity was also well simulated. On the basis of correlations with two major reanalysis datasets, the simulation fairly reproduced realistic day-to-day variations of atmospheric fields. Day-to-day variations of zonal wind showed strong and weak monsoon westerly phases. Because monthly mean precipitation is associated with various atmospheric conditions, such as strong and weak monsoon westerly phases, a three-year experiment can allow for discussion of the potential impact of LUCCs.

The simulated atmospheric structure was examined, compared with the 6-hourly soundings observed at Ubon Ratchathani (104.87 °E, 15.25 °N), Thailand. The vertical structure of virtual potential temperature was well simulated, compared with the observations (Figure 3). The simulated heights of the boundary layer at 1200 local time (LT) on 5 September and 8 September 1998 were also consistent with the observed heights. The height of the planetary boundary layer was approximately 1000 m at 1200 LT. Boundary layer heights on other days were also well simulated (not shown). The vertical structures of water vapour were simulated as well, although the absolute values were sometimes overestimated in the model (not shown). The consistency of the boundary layer heights and the vertical structure of water vapour imply that sensible and latent heat fluxes from the surface were realistically simulated. The simulated vertical

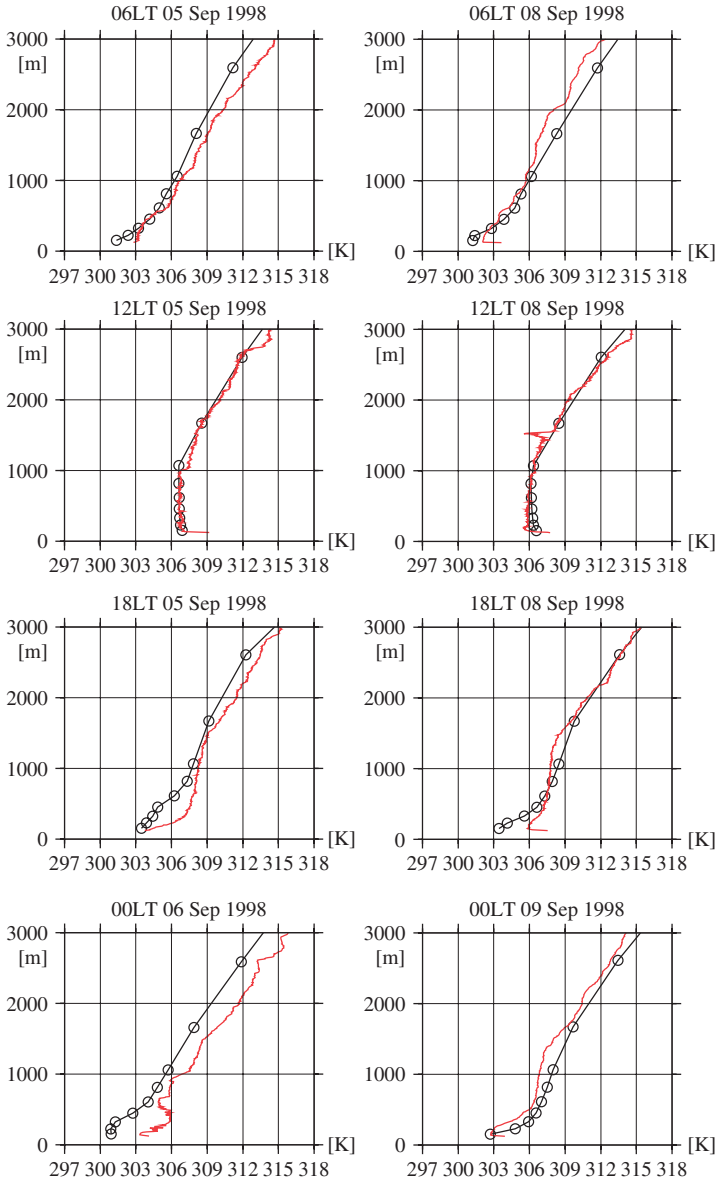

Figure 3. The vertical structure of virtual potential temperature on 5 and 8 September 1998 at Ubon Ratchathani (104.87 °E, 15.25 °N), Thailand. Black lines indicate the simulation. The open circles denote the vertical distribution of terrain-following levels in the model. Red lines represent observations.

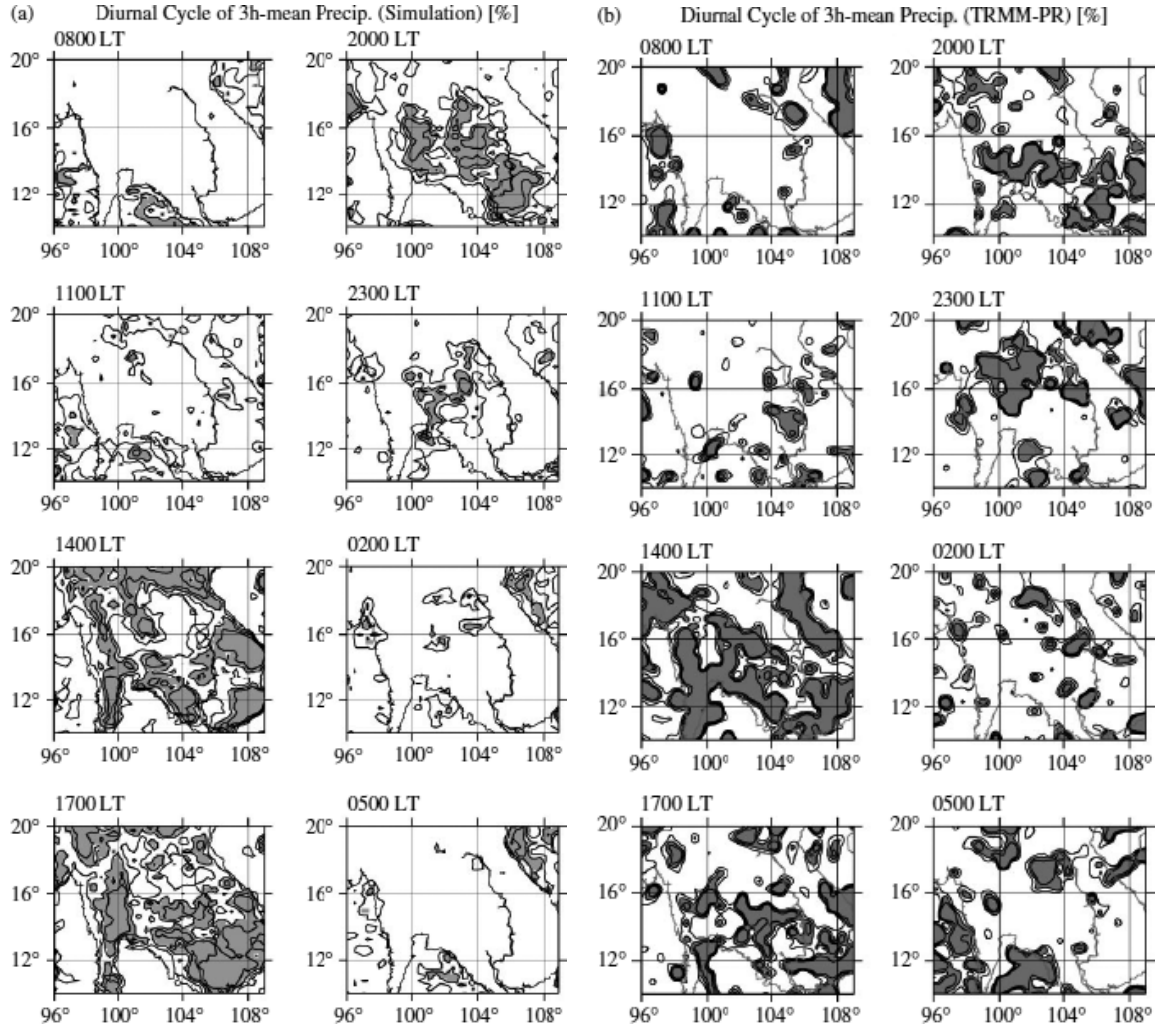

Figure 4. The contribution rate to the total precipitation (a) of three-year (1998–2000) simulated precipitation for September and (b) of eight-year (1998–2005) climatological precipitation for September observed by TRMM-PR. This contribution rate is defined as the proportion of rainfall during a 3-h period to the total rainfall amount for 24 h.

structures of virtual potential temperature at 1800 LT sometimes differed from the observations, probably due to the nonlinear behaviour of mesoscale convective systems.

Previous studies have noted that diurnal variations of precipitation dominate over and around the Indochina Peninsula (Satomura, 2000; Ohsawa *et al*., 2001; Hirose and Nakamura, 2005; Takahashi *et al*., 2010). Therefore, we also examined the reproducibility of diurnal variation of precipitation by looking at 3-h mean diurnal precipitation variations. To facilitate the examination of the diurnal pattern of precipitation, the contribution rate is shown in Figure 4 because the total amount of precipitation of TRMM-PR was somewhat smaller than simulated values. The contribution rate is defined as the proportion of rainfall during a 3-h period to the total rainfall amount for 24 h at each grid point. The value at 1400 LT, for example, indicates the mean precipitation from 1300 to 1559 LT. The three-year diurnal variations of the simulated precipitation for September and the eight-year mean diurnal variations of TRMM-PR precipitation are shown in Figure 4.

Daytime precipitation was simulated over the mountain ranges and along the coasts [Figure 4(a)]. Evening precipitation began at 1700 LT over low-altitude land areas such as Bangkok, Thailand and a plain in Cambodia. Over the southern Khorat Plateau, precipitation had a diurnal cycle with a peak at 2200 LT, lasting until early morning. This simulated diurnal pattern of precipitation [Figure 4(a)] was similar to that of TRMM-PR [Figure 4(b)]. Thus, the diurnal pattern of precipitation was fairly simulated, which indicated that CTL can be considered to have reproduced diurnal variations of precipitation over and around the Indochina Peninsula.

3.2. Differences among CTL, WET and DRY

The purpose of this study was to understand the impacts of surface condition changes on precipitation. With this goal in mind, this section discusses the differences in precipitation among the three sensitivity experiments. Because the effects of surface condition change may depend on environmental circulation, we averaged the simulated results for September over three years for each experiment.

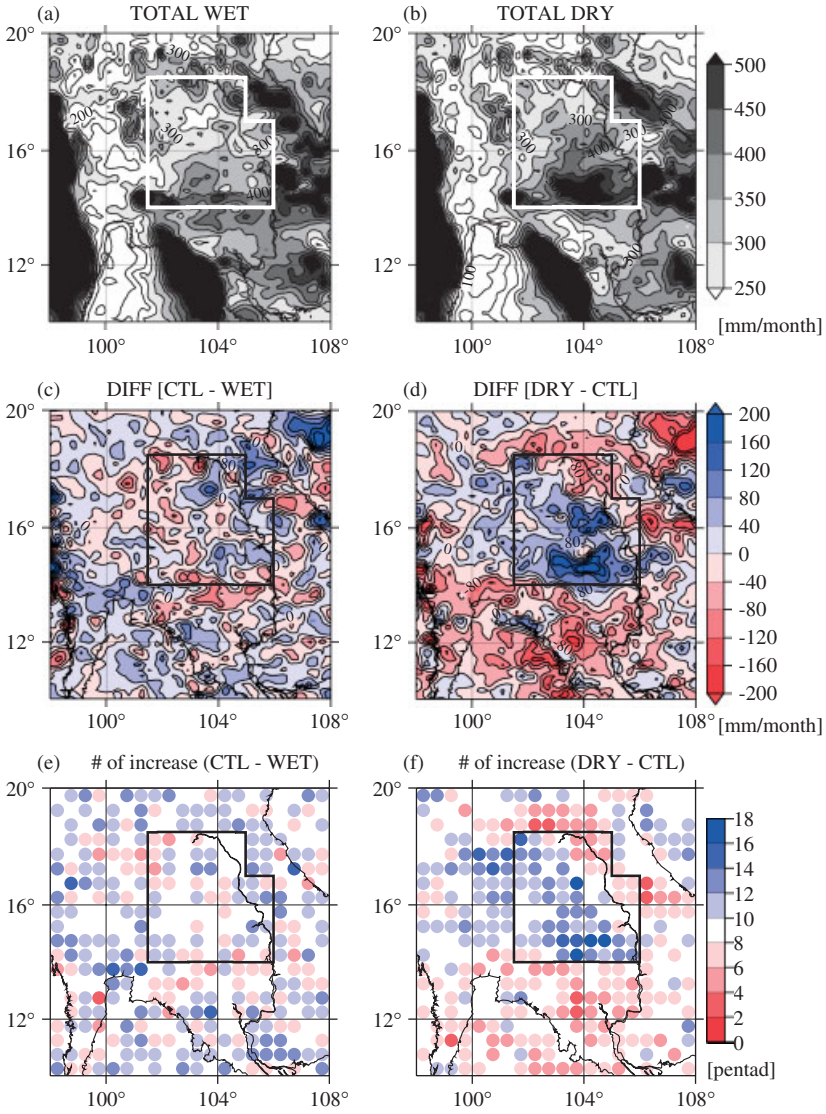

Figure 5. Total amount of monthly precipitation of (a) WET and (b) DRY. Differences in monthly precipitation (c) between DRY and CTL (CTL−WET) and (d) between CTL and DRY (DRY−CTL) are shown. The numbers of pentads out of 18 that calculate increase in pentad precipitation (e) between DRY and CTL (CTL−WET) and (f) between CTL and DRY (DRY−CTL) are shown. The calculation period of each experiment is three months, which is 18 pentads (90 days). The numbers of pentads that show increase in precipitation were counted at each half-degree grid. White and black lines indicate the disturbed region.

Figure 5(a) and (c) shows that the total precipitation in the CTL experiment was greater than that of WET over the southern Khorat Plateau (around 104 °E, 15°N, within the disturbed region) and slightly less south of the Khorat Plateau (around 104 °E, 13°N, outside the disturbed region). Although the area mean total precipitation of CTL was almost the same as that of WET over the disturbed region, the change in surface conditions altered the spatial distribution of precipitation around the southern boundary between the disturbed and undisturbed regions [Figure 5(a)].

To investigate the impact of severe deforestation, we conducted the DRY experiment. Compared with CTL, DRY showed an increase in precipitation over the disturbed region, particularly over the southern Khorat Plateau [104 °E, 15°N, Figure 5(d)]. However, precipitation decreased in the area surrounding the disturbed region, particularly to the south of the Khorat Plateau (104 °E, 13°N, outside the disturbed region). The spatial distribution of precipitation also differed between CTL and DRY [Figure 5(b) and (d)]. Among the three experiments, signals of precipitation differences were found over and around the disturbed regions.

To investigate the robustness of the increases in precipitation over the disturbed region between the sensitivity experiments and CTL, we show the spatial distribution of the number of pentads out of 18 in which increased precipitation was calculated. Each experiment was conducted for three months, and each experiment had 18 pentads (90 days). Large numbers indicate that precipitation increased in various atmospheric conditions, such as in the strong and weak monsoon westerly phases. If a few unusual precipitation events contributed to the increase in precipitation, the number should be small.

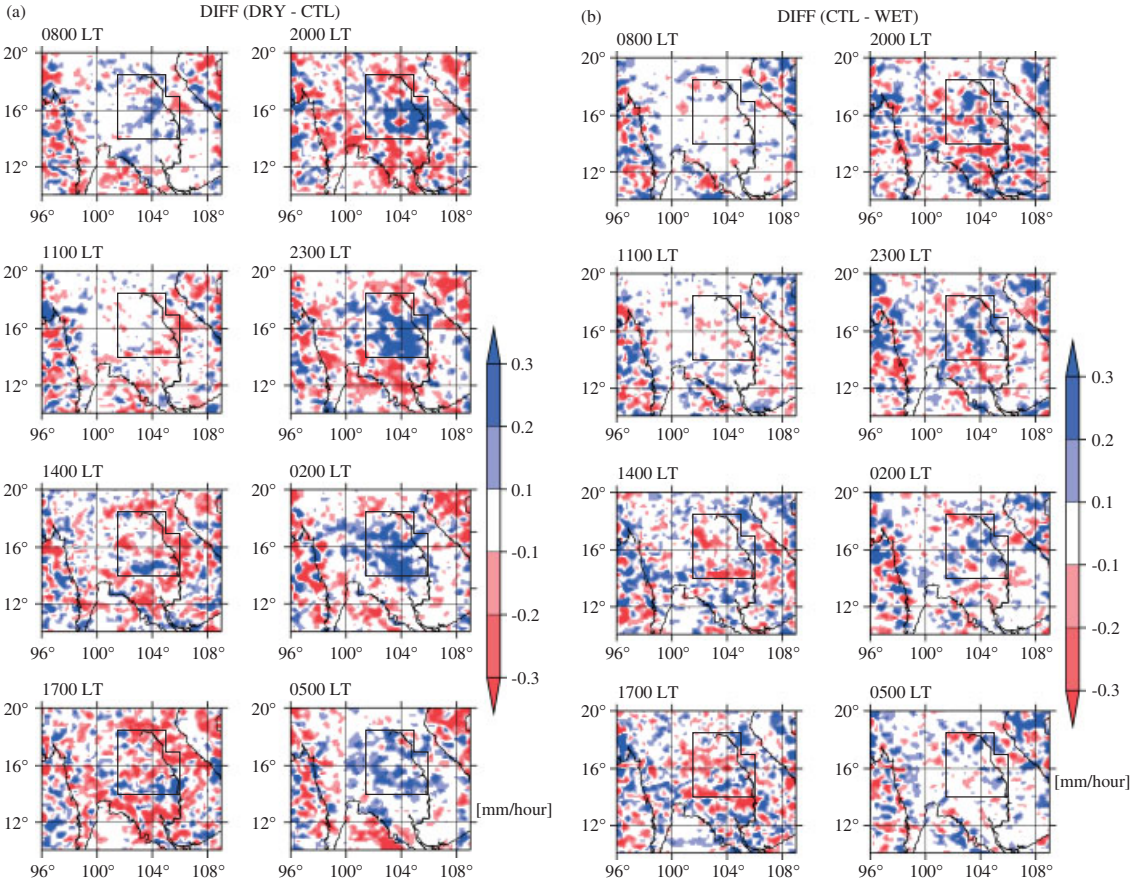

Figure 6. Difference in the September mean diurnal cycle in precipitation over three years (a) between DRY and CTL (DRY−CTL) and (b) between CTL and WET (CTL−WET).

Thus, the pentad number can be used to investigate the robustness of the mean difference in precipitation. Larger numbers of pentads appear over the regions where increases in precipitation were found [Figure 5(e) and (f)]. This result indicated that the increases in precipitation over the disturbed region were calculated under various atmospheric conditions. Therefore, the signals are robust and indicate that changes in the surface conditions can locally alter the spatial distribution of precipitation.

Note that the three experiments not only showed an association between a drier surface condition and likely increases in precipitation over the disturbed region but also showed decreases in precipitation in areas around that disturbed region. Interestingly, there was no large difference between WET and CTL. However, CTL and DRY showed large precipitation differences over the disturbed region, as will be discussed in Section 4.

As noted previously, the CTL experiment reproduced the diurnal pattern of precipitation. Because changes in precipitation may be closely associated with basic precipitation processes in the region, this subsection also discusses changes in the diurnal pattern of precipitation due to changes in the surface condition.

Figure 6(a) presents changes in precipitation from CTL to DRY during each time period. Increased precipitation was calculated from evening to morning over the disturbed region, whereas small changes in daytime precipitation were also found in the disturbed region. The timing of increased precipitation over the Khorat Plateau coincided with the climatological peak in the diurnal precipitation cycle of the region. The differences seemed to be associated with the climatological diurnal cycle of precipitation. Thus, the sensitivity experiment indicated that the diurnal cycle of precipitation was more marked in DRY compared with CTL.

A similar tendency was found for the difference between CTL and WET [Figure 6(b)], although the signal was weaker than that between CTL and DRY. Nocturnal precipitation was also increased over the disturbed area. These sensitivity experiments suggest that diurnal variation in precipitation is likely the key process for understanding the mechanism of precipitation changes responsible for the surface condition changes over northeast Thailand. Therefore, the following subsection investigates characteristics of precipitation from evening to morning over northeast Thailand.

3.3. Climatological diurnal cycle of precipitation over northeast Thailand

To investigate the atmospheric circulation fields associated with the diurnal cycle of precipitation, we examined the diurnal component of water vapour flux and

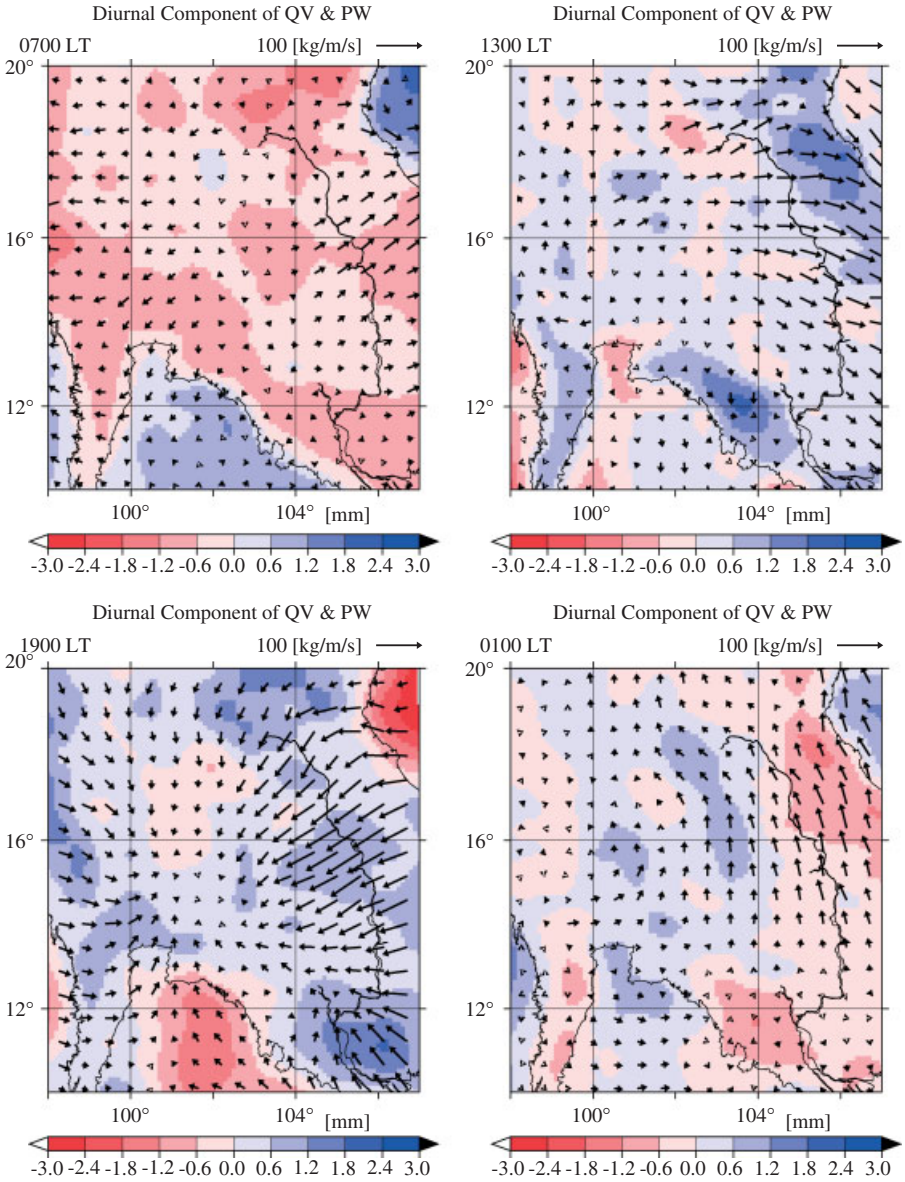

Figure 7. The monthly mean diurnal cycle of vertically integrated water vapour flux (vector) and precipitable water (colours) of CTL over three years for 0700, 1300, 1900 and 0100 LT. The diurnal component is shown.

precipitable water. The diurnal component was calculated as the monthly daily mean subtracted from the monthly mean diurnal cycle.

The diurnal variation in precipitable water (Figure 7) was consistent with that of precipitation (Figure 4). Water vapour was transported to the mountain ranges at 1300 LT, probably in association with thermally induced local circulation. The increase in water vapour over the mountain ranges was consistent with daytime convective activity there. Along the coasts, the sea breeze probably transported water vapour from the sea to the coast during daytime. At 1900 LT, water vapour fluxes from the Annam Mountain range and the Gulf of Thailand met at the southern Khorat Plateau. The increase in precipitable water from evening to midnight (0100 LT) was consistent with the heavy nocturnal precipitation over the Khorat Plateau. The water vapour over land was gradually transported to the adjacent sea by 0700 LT.

Because the Indochina Peninsula is located in the tropics, it receives enough energy for the development of convective activity. Much water vapour is probably also supplied from adjacent seas. These conditions favour the development of convective activity in daytime. However, the convective activity of the Khorat Plateau is suppressed during daytime, implying the possible existence of a suppression mechanism. To understand the suppression of convective activity during daytime, a vertical–longitudinal cross-section of vertical wind along 17°N is shown in Figure 8. Ascending motion developed along the mountain ranges from 1000 to 1600 LT (1300 LT is shown in Figure 8), whereas descending motion was simulated over the Khorat Plateau (102°–104°E). The descending motion was likely induced by the thermally induced local circulations and a compensating downward motion, coupled with the convective activities over the mountain ranges. Daytime convective activity

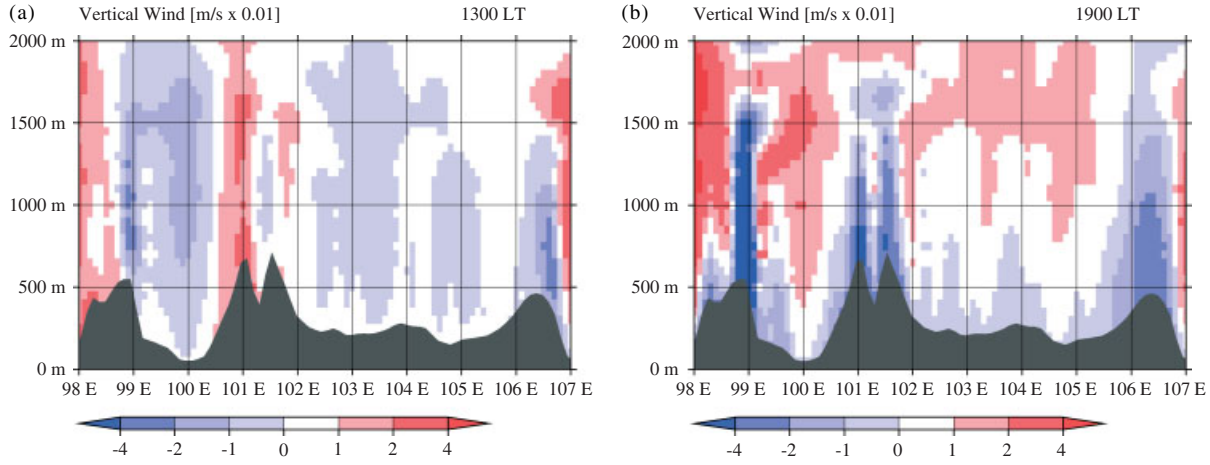

Figure 8. Vertical–longitudinal cross-section of monthly mean vertical wind of CTL over three years along 17°N for 1300 LT (a) and 1900 LT (b). The red colour indicates ascending motion, whereas the blue colour denotes descending motion. The grey mask indicates terrain.

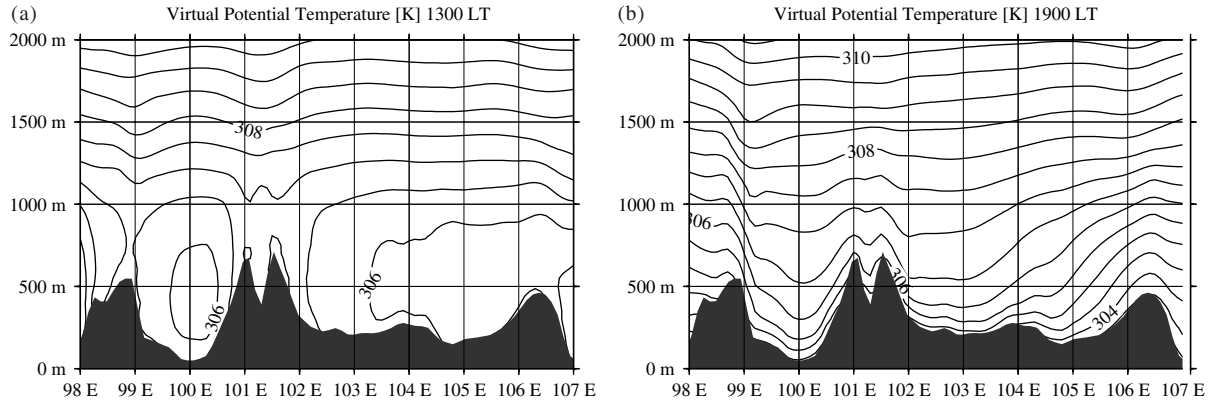

Figure 9. Vertical–longitudinal cross-section of monthly mean virtual potential temperature of CTL over three years along 17°N for 1300 LT (a) and 1900 LT (b). The grey mask indicates terrain.

over the Khorat Plateau was probably suppressed by this descending motion. In addition, some water vapour was transported to the surrounding mountain regions, a process that may also have supported suppression through the decrease of potential convective instability. By 1900 LT, the downward motion weakened because of the absence of convective activity over the mountain ranges and the alternation of local winds from anabatic winds to katabatic ones. The absence of descending motion can produce an atmospheric structure in which convective activity can develop.

Figure 9 shows a vertical–longitudinal cross-section of virtual potential temperature. The convective boundary layer was developed over the Khorat Plateau during daytime [Figure 9(a)]. The structure of virtual potential temperature favoured the development of anabatic winds, which probably formed convective activity along the mountain ranges. During nighttime, the isothermal lines followed the terrain, favouring the formation of katabatic winds [Figure 9(b)].

Figure 10 shows the diurnal components of wind at 10 m above the surface. Winds converged over the mountain ranges at 1300 LT [Figure 10(a)]. Thermally induced circulations were strong near the coast, a phenomenon that can be explained by the superposition of mountain–valley and land–sea breezes. After sunset, strong downslope winds were simulated along the western side of the Annam Mountain ranges [1900 LT, Figure 10(b)]. Westward winds also developed over the central Khorat Plateau. The climatological characteristics of the diurnal variations of low-level wind fields were consistent with those of virtual potential temperature. The katabatic winds from the Annam Mountains flowing into the Khorat Plateau at 1900 LT possibly triggered convective activity. However, the intensification of downslope winds from the Annam Mountains may not be explained solely by radiative cooling of the slope after sunset. Rather, part of the intensification may be related to the moist processes of convective activity. Because the moist processes of mesoscale convective systems are, in general, highly nonlinear, it is not possible to identify the mechanisms of the triggers and developments of convective activities from climatological mean fields. Thus, we investigated typical cases of the development of nocturnal precipitation over the Khorat Plateau. Analysis of two typical cases is presented in the following subsection.

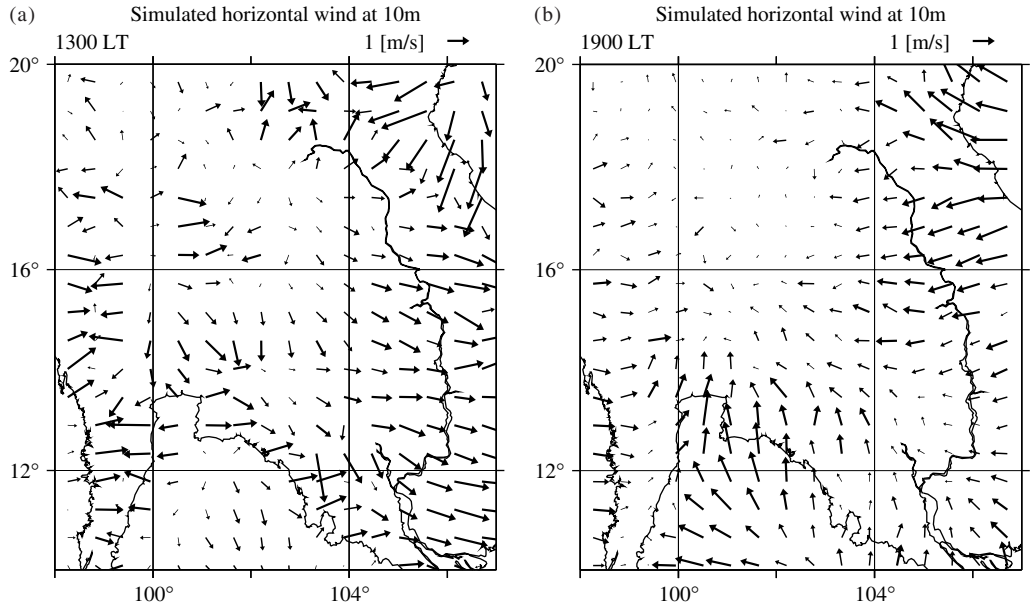

Figure 10. September mean diurnal component of the horizontal wind pattern at 10 m above the surface of CTL over three years for 1300 LT (a) and 1900 LT (b).

3.4. Mechanism of nocturnal precipitation over the Khorat Plateau

Previous subsections have described the climatological diurnal pattern in precipitation and the associated atmospheric circulations. The climatological analysis suggested that nocturnal precipitation was likely associated with downslope wind from the mountains surrounding the Khorat Plateau (Figure 10). However, the essential mechanism of nocturnal precipitation systems over the Khorat Plateau requires further clarification. This subsection investigates that mechanism.

Two cases were chosen that are typical in terms of similarity of the diurnal pattern of precipitation to the climatological diurnal pattern of precipitation. In the first case, a strong monsoon westerly prevailed over the Indochina Peninsula on 1 September 1999. In the second case, on 23 September 1999, the monsoon westerly was weak. Figure 11 shows the diurnal sequences of precipitation for these two cases, which were similar to the climatological diurnal pattern of precipitation (Figure 4).

Figure 12 presents the vertical section of moist static energy (contours), winds (vectors), precipitation (open black bar in each lower panel) and virtual potential temperature (shading) along the grey-dashed line in Figure 1(a). The vectors show the horizontal wind velocities along the section and vertical wind velocities. Moist static energy is given in Kelvin. The accumulated precipitation, shown as an open black bar in the lower panels, was totalled from the current time (shown at the upper left of the upper panel) to 30 min later.

The convective boundary layer gradually developed over land, particularly over the Khorat Plateau after sunrise (not shown). Anabatic winds met over the crests of the western and eastern mountain ranges of the Khorat Plateau, inducing convective activities at 1500 LT. A cold air mass was formed on top of the mountain ranges, possibly as a result of convective activities. Descending motions were shown over the Khorat Plateau. The cold air mass drifted into the basin-shaped Khorat Plateau from 1600 to 1900 LT. Gravity-current-like flow probably triggered convection at the eastern slope of the mountain ranges at 102.5 °E at 1800 LT. The induced convective activity could further form the cold air mass (2100 LT) and likely result from the evaporation of raindrops and from raindrops carrying down low moist static energy air from above the planetary boundary layer. A cold air mass seemed to induce convection in sequence (not shown).

As a result of these processes, the simulated precipitation system over the Khorat Plateau moved eastward. Similar systems repeated during the night. In addition, similar gravity-current-like flow formed on the western slope of the Annam Mountain range although the induced precipitation was relatively weaker.

On 23 September 1999 (Figure 13), a precipitation system was developed on the western slope of the mountain ranges of 106 °E at 1400 LT (not shown). A cold air mass was formed on the western slope of the mountain range and drifted westward into the Khorat Plateau (1800 and 1900 LT). The cold air mass, associated with a westward-travelling precipitation system, extended to 104 °E in the Khorat Plateau at 2100 LT. This westward flow was also likely to be a gravity current, and the cold air mass probably triggered the convective systems around 104 °E. The system moved westward. The formation mechanism of this cold air mass seems to have been similar to that of the precipitation system on 1 September 1999. In this manner, moist convective processes intensified the katabatic winds from the mountain ranges. The cold air mass that resulted from convective activity probably enhanced the katabatic winds.

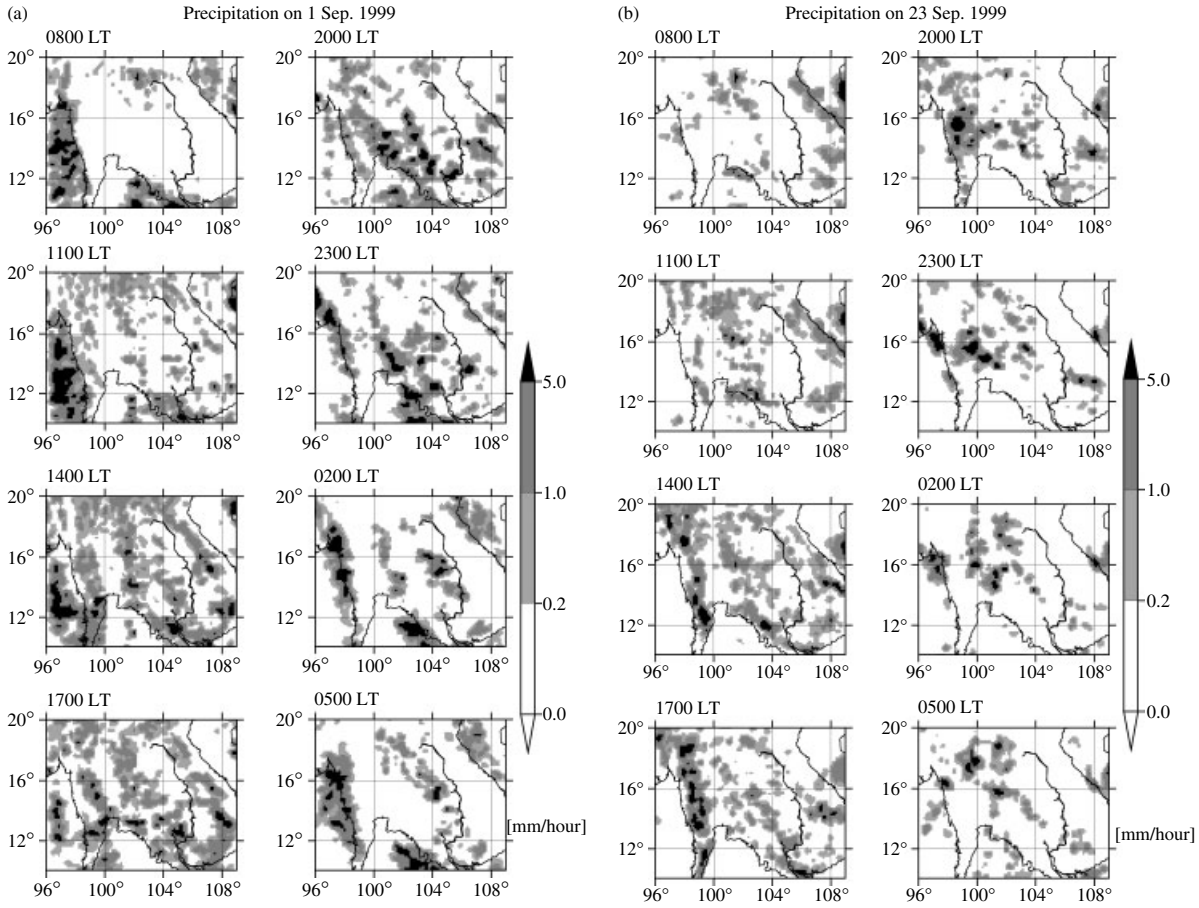

Figure 11. Diurnal sequence of 3-h precipitation of CTL for each time period (a) on 1 September 1999 and (b) on 2 September 1999.

Both eastward and westward migrations of precipitation systems were identified. The examination of relationship of these systems to the low-level monsoon westerly indicated that eastward-migrating systems prevailed during the westerly phases. However, some westward migrations were also found when the westerly prevailed. During weak monsoon westerly phases, more westward migrations were indentified. Other days showed similar convective systems during nighttime. Basically, the precipitation system in this area was associated with the low-level monsoon westerlies. During the monsoon season, more eastward-migrating precipitation systems were simulated. These simulated convective systems were likely consistent with the two-dimensional cloud-resolving modelling results of Satomura (2000). This result was also consistent with recent findings by Oouchi *et al*. (2009), who used a global cloud-resolving model.

4. Discussion

4.1. Diurnal variations in water vapour modulated by surface condition change

A pronounced increase in precipitation during nighttime was shown due to changes in the surface condition from CTL to DRY. Because of this large sensitivity experiment signal, we investigated the differences between CTL and DRY. The area-averaged precipitation over the disturbed area was 323.9 mm/month in CTL and 366.0 mm/month in DRY. Precipitation may have increased due to a larger number of precipitation events, or it may have increased with an increase in precipitation intensity rather than in precipitation frequency. How do we explain the increase? In this study, we did not consider the life cycle of precipitation events. Thus, precipitation frequency coincided with the duration of precipitation. We examined changes in the frequency by counting precipitation events, defined by certain criteria. The mean precipitation intensity of CTL, $\overline{P}$, was 0.45 mm/h. The changes in the frequency of precipitation events of more than 0.1, 0.22 and 0.45 mm/h were 2.3%, 2.7% and 3.9%, respectively (Table II). Although the frequency of precipitation may have increased somewhat, these changes would not explain the 13% increase in total September precipitation. Therefore, increased mean precipitation intensity was probably the main reason for the increase in total precipitation. In general, the change shown in each individual precipitation event cannot reflect the climatological change in precipitation because of the nonlinearity of precipitation events. To understand the increase, we examined changes in the climatological diurnal cycles of winds and water vapour fields.

The differences in temperature at 2 m and winds at 10 m between CTL and DRY showed that the temperature of DRY was much higher than that of CTL

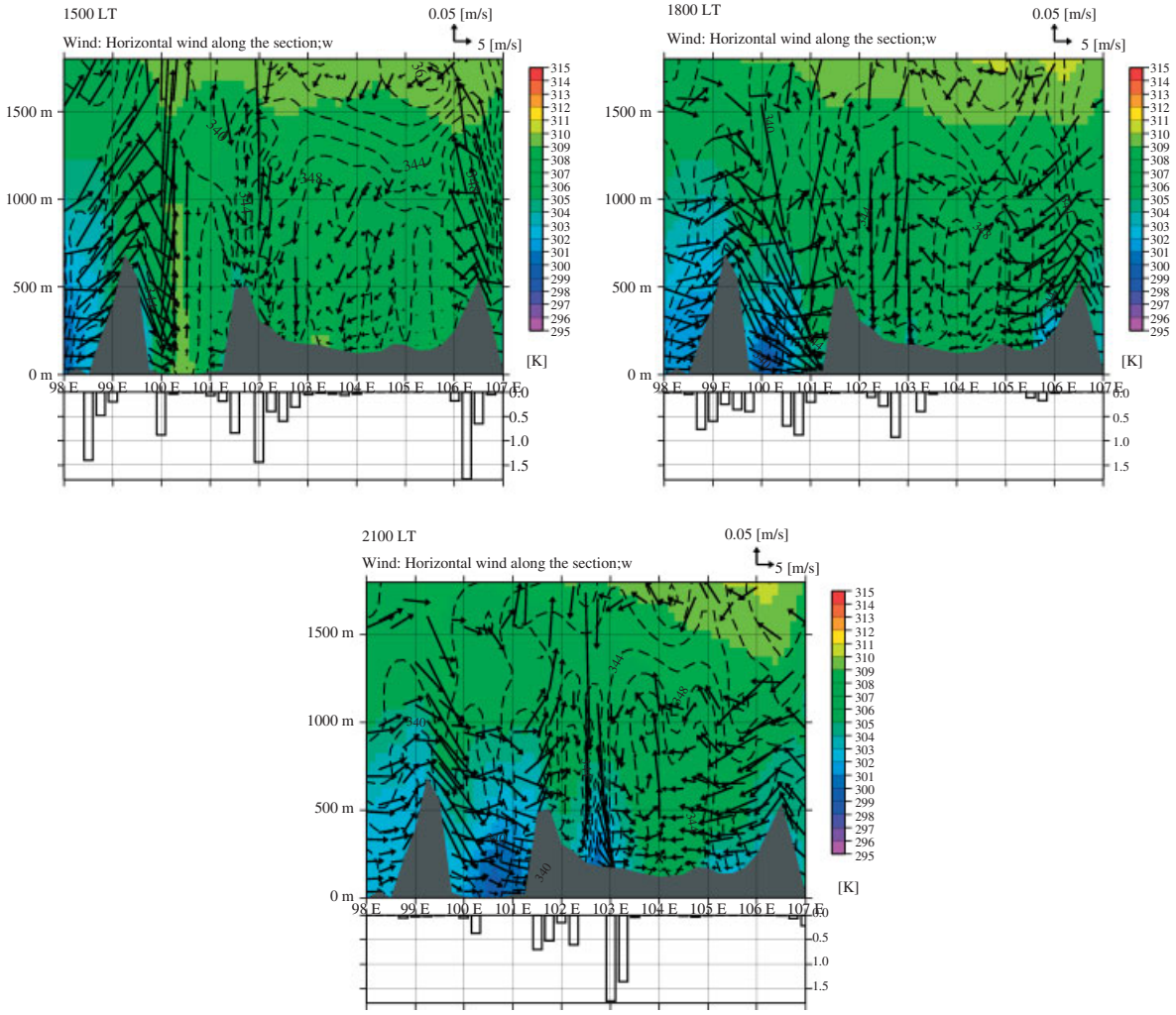

Figure 12. Vertical section moist static energy (dashed lines) and virtual potential temperature (shading) and winds in each upper panel and precipitation in each lower panel of CTL along the grey-dashed line in Figure 1(a) for 1500, 1800 and 2100 LT of 1 September 1999. The vectors show horizontal wind along the section and vertical velocity. The bars in each lower panel denote accumulated precipitation was totalled from the current time (shown at the upper left of the upper panel) to 30 min later. The accumulated precipitation is shown in the right vertical axis. The unit of the accumulated precipitation is millimetre. The grey mask indicates terrain. The vectors at upper right-hand corner indicate the lengths of horizontal and vertical velocities, 0.05 and 5 m/s, respectively.

(Figure 14). The difference in near-surface temperature along the boundary between the disturbed and undisturbed regions in DRY induced local circulations. Wind convergence was identified over the disturbed region. The convergence in wind possibly enhanced the convective activity and precipitation. However, the precipitation increase due to the assumed surface condition change of extreme deforestation was distinct during nighttime. The difference in 10-m wind also indicated wind convergence at 1300 LT (not shown). Nevertheless, no increase in daytime precipitation was found (Figure 6). The wind convergence did not directly explain the increase in precipitation.

We also examined the modulated diurnal variations of water vapour fields (Figure 15). The difference in precipitable water during each time period showed a decrease from late morning to evening and an increase from late evening to early morning. The decrease in precipitable water in daytime was likely responsible for the decrease of evapotranspiration from the surface because the difference in evapotranspiration from the

Table II. The simulated precipitation of CTL and DRY, area-averaged within the disturbed region (Figure 1).

Category	Precip (mm/month)	Freq >0.1	Freq $>0.22\ \overline{P}/2$	Freq $>0.45\ \overline{P}$
CTL	323.9	32.75	25.79	19.38
DRY	366.0	33.51	26.48	20.13
Increase (%)	13.0	2.3	2.7	3.9

The unit of precipitation is mm/month.
The frequency of precipitation was defined as the frequency at which accumulated precipitation for 3 h in each grid exceeded threshold values, set at 0.1, 0.22 and 0.45 mm/h.
The value of 0.45 mm/h was the averaged intensity of precipitation $\overline{P}$ for CTL.
The bottom line denotes the increase rate of each parameter from CTL to DRY.

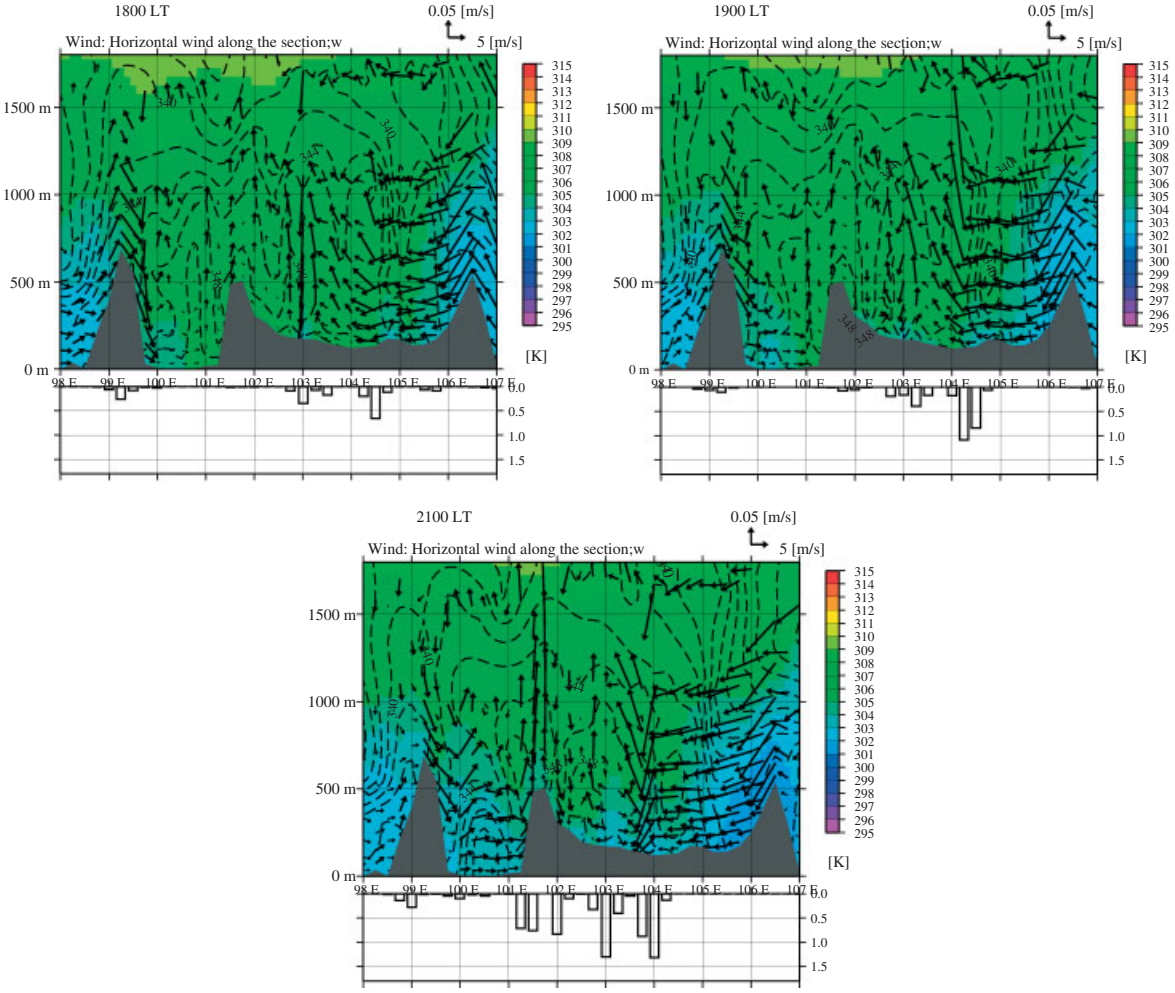

Figure 13. As in Figure 12 except for 1800, 1900 and 2100 LT of 23 September 1999.

surface between DRY and CTL was comparable with the decrease in precipitable water. The timing of the drastic increase in precipitable water during the night corresponded to the increase in precipitation due to the surface condition change from CTL to DRY. The modulated pattern of water vapour flux was correlated with that of 10-m winds, indicating that the thermally induced winds altered the diurnal cycle of precipitable water. Note also that the phase of diurnal variations of the modulated precipitable water was synchronized with the climatological phase of the diurnal cycle of water vapour. Once a precipitation system occurs over the Khorat Plateau during nighttime, larger amounts of precipitation can fall due to the increased precipitable water. The thermally induced local circulation modulates the diurnal cycle of precipitable water over and around the disturbed region. However, the enhancement of water vapour convergence may not be solely explained by thermally induced circulation. Enhanced convection over the disturbed region may lead to more water vapour around the convection. The two mechanisms may interact and enhance each other. The modulated diurnal variations of water vapour can explain the increase in precipitation. The daytime decrease of precipitable water was not

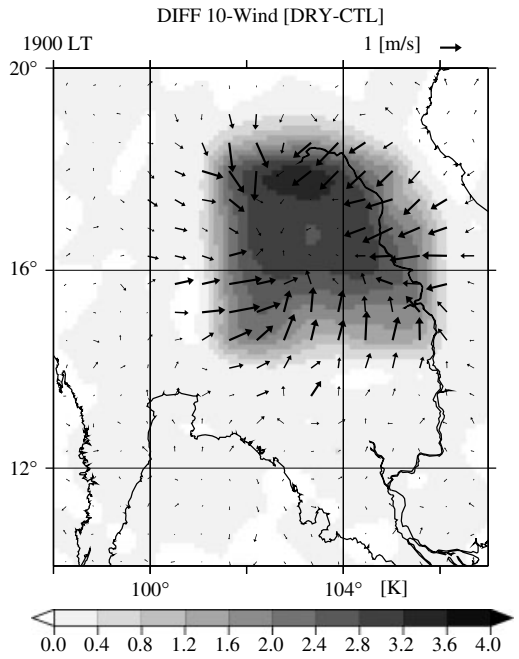

Figure 14. Difference in monthly mean diurnal pattern of winds at 10 m above the surface over three years between DRY and CTL (DRY−CTL) for 1900 LT.

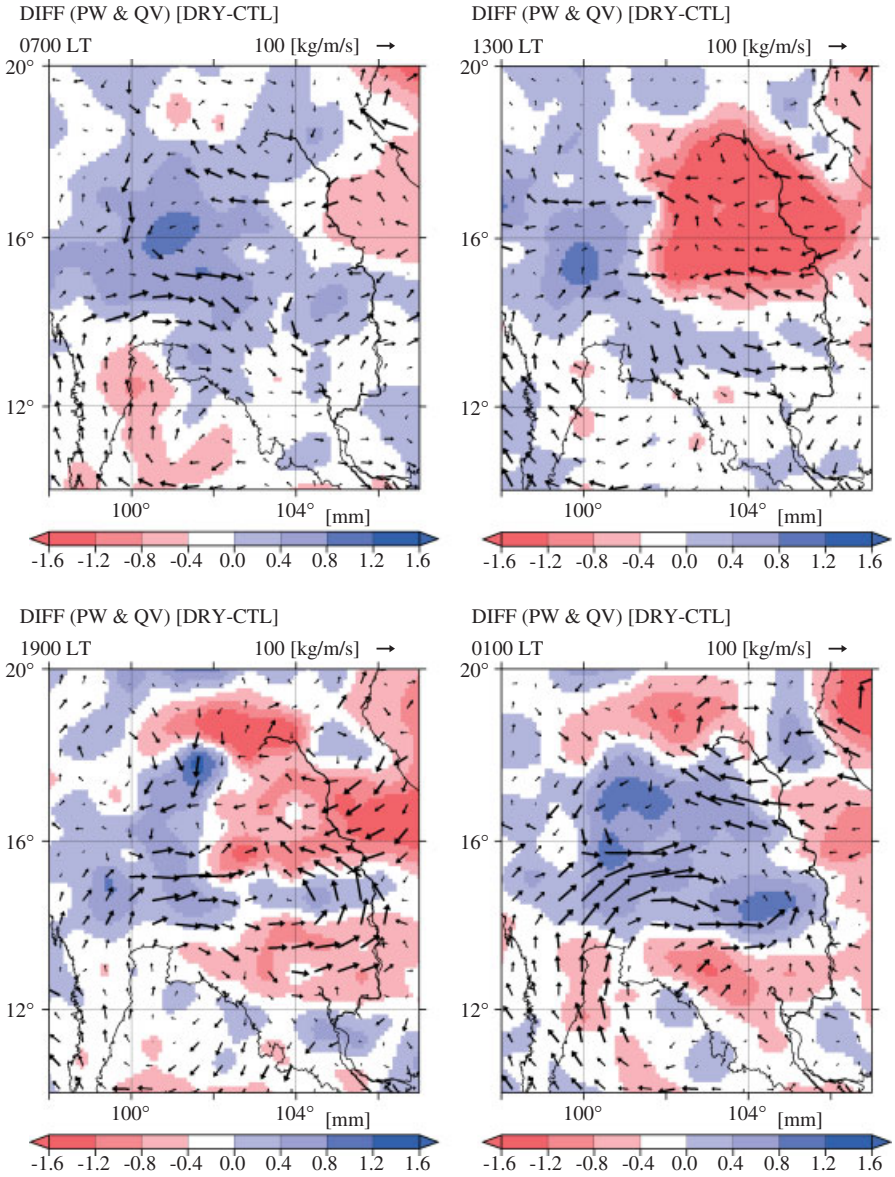

Figure 15. Difference in the monthly mean diurnal cycle of vertically integrated water vapour flux (vector) and precipitable water (colours) over three years between DRY and CTL (DRY−CTL) for 0700, 1300, 1900 and 0100 LT.

strongly associated with daytime convective activities because daytime convection over the Khorat Plateau was not climatologically active (Figure 16). Although the daily mean precipitable water of DRY was lower than that of CTL (Figure 16), the modulated amplitude of precipitable water may nonlinearly affect precipitation systems.

The signal of WET was much weaker than that of DRY, compared with CTL. Table III shows the area mean sensible heat flux, latent heat flux from the surface, Bowen ratio and temperature at 2 m above the surface. The difference in Bowen ratios was large between DRY and CTL but small between WET and CTL. Changes in surface flux from WET to CTL were smaller than those from CTL to DRY, which likely resulted in weaker thermally induced local circulations and smaller changes in precipitation in WET.

4.2. Observed long-term decrease in precipitation

This study investigated the potential impact of LUCCs over northeast Thailand on the Indochina Peninsula. One motivation of this study was Kanae *et al.*'s (2001) finding that the observed decrease in precipitation in this region may be explained by regional-scale LUCCs. On the basis of observational and numerical modelling studies, Takahashi and Yasunari (2006, 2008) and Takahashi *et al.* (2009) reported that concurrent changes in tropical cyclone activity can explain the observed decrease in precipitation. Furthermore, our study suggested that an increase in precipitation was responsible for the changes from the wet to dry surface conditions. Our results disagree with those of Kanae *et al.* (2001). Kanae *et al.* (2001) used a 60-km mesh, which would not have been fine enough to resolve local circulations and may have led to the discrepancy between their study and ours. Another large difference involves whether CCP was used;

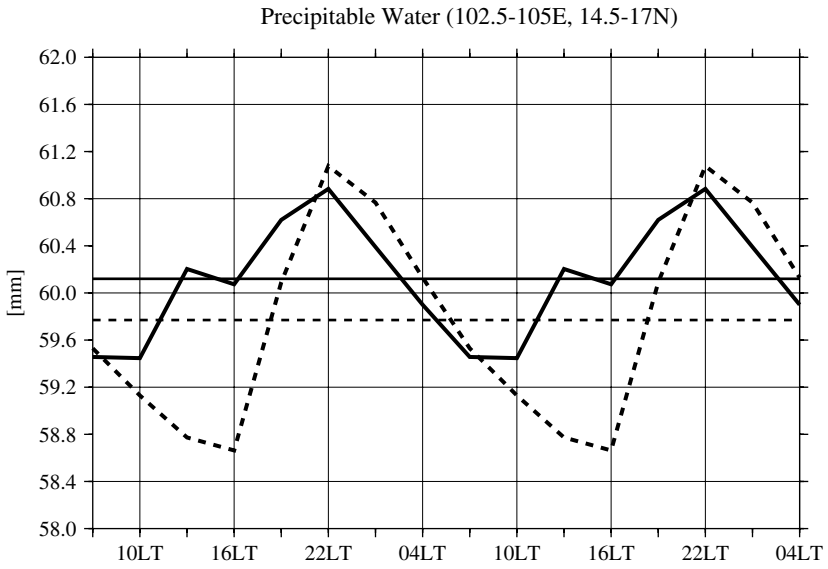

Figure 16. The monthly mean diurnal cycle of precipitable water of DRY (dashed) and CTL (solid) over three years. The precipitable water was domain averaged within an area at 102.5°–105 °E, 14.5°–17°N where increase of precipitation was due to the changes in land surface condition from CTL to DRY. Their daily mean values were also shown. The unit is millimetre.

Table III. The simulated sensible heat flux H, latent heat flux LE from the surface, Bowen ratio Bo and temperature at 2 m T_{2m} at 1300 LT of WET, CTL and DRY, area-averaged within the disturbed region (Figure 1).

Category	H (W/m^2)	LE (W/m^2)	Bo	T_{2m} (K)
WET	81.3	302.7	0.27	301.6
CTL	113.8	274.9	0.41	302.2
DRY	257.1	131.1	1.96	304.5

CCP strongly affects the reproduction of the diurnal cycle of precipitation, even if local circulation is almost simulated (Hara *et al*., 2009). Hence, the observed long-term decrease in precipitation during the latter half of the last century cannot be explained by the effects of LUCCs.

5. Conclusions

This study investigated the potential impact on regional climate of LUCCs in northeast Thailand (Khorat Plateau), in terms of diurnal variations of precipitation, using a high-resolution regional climate model. Northeast Thailand, which was once widely covered by tropical rainforest, has been intensively deforested over the past century. Currently, most land in northeast Thailand is used for cultivation.

Comparison of CTL with observations showed that the simulation captured the spatial distribution of the total amount of precipitation over and around the Indochina Peninsula. The simulated height of the planetary boundary layer and vertical structure of water vapour also corresponded to the observations, indicating that CTL reproduced realistic sensible and latent heat fluxes from the surface. CTL also reproduced realistic diurnal variations of precipitation, showing a peak over the Khorat Plateau from evening to midnight.

Two sensitivity experiments were conducted with different soil moistures and vegetation densities. Compared with the CTL experiment, WET (DRY) showed less (more) precipitation, less (more) sensible heating, more (less) latent heating and lower (higher) surface temperature over the converted region. Thus, a drier surface condition increased precipitation in the study area. Note that distinct changes in precipitation due to LUCCs were found during nighttime over the Khorat Plateau. Because nocturnal precipitation is dominant in this area, the changes are closely tied with climatological diurnal variations of precipitation over the Indochina Peninsula region.

Over northeast Thailand during daytime, a weak downward flow was formed, which was probably caused by the thermally induced local circulation and a compensating downward motion associated with the convective activity over the surrounding mountain ranges. During the evening, the structure of virtual potential temperature changed, and katabatic winds were developed from the surrounding mountain ranges to the Khorat Plateau. Case studies showed that daytime convection formed a cold-air-mass-like cold pool over the mountain ranges; this pool drifted into the basin-shaped Khorat Plateau and induced convective activity in evening. The flow seemed to be a gravity current. The induced convection further formed the cold air mass, which in turn developed convection. Consequently, the precipitation systems moved into the Khorat Plateau. The climatological nocturnal precipitation over the Khorat Plateau consisted of the repeatable formation of convective systems.

The increase of total precipitation due to the LUCC over the converted region was associated with diurnal

variation of water vapour flux. Climatologically, the diurnal peak in precipitation was from evening to early morning over the Khorat Plateau. The drier condition intensified diurnal variation of precipitable water associated with the thermally induced local circulation responsible for the horizontal gradient of surface conditions. That is, more water vapour was supplied to the Khorat Plateau during nighttime. The modulated diurnal variation of precipitable water due to the LUCC synchronized with the climatological diurnal cycle of precipitation, which can explain the increase in total precipitation.

Acknowledgements

This work was partly supported by the Global Environment Research Fund (B-061) and (B-092) of the Ministry of the Environment, Japan.

References

Brovkin V, Claussen M, Driesschaert E, Fichefet T, Kicklighter D, Loutre M, Matthews H, Ramankutty N, Schaeffer M, Sokolov A. 2006. Biogeophysical effects of historical land cover changes simulated by six Earth system models of intermediate complexity. *Climate Dynamics* **26**(6): 587–600.

Chase T, Pielke R Sr, Kittel T, Nemani R, Running S. 2000. Simulated impacts of historical land cover changes on global climate in northern winter. *Climate Dynamics* **16**(2): 93–105.

Chen F, Dudhia J. 2001. Coupling an advanced land surface – hydrology model with the Penn State – NCAR MM5 modeling system. Part I: model implementation and sensitivity. *Monthly Weather Review* **129**(4): 569–585.

Dai A. 2006. Precipitation characteristics in eighteen coupled climate models. *Journal of Climate* **19**(18): 4605–4630.

Dai A, Trenberth K. 2004. The diurnal cycle and its depiction in the community climate system model. *Journal of Climate* **17**(5): 930–951.

D'Almeida C, Vorosmarty C, Hurtt G, Marengo J, Dingman S, Keim B. 2007. The effects of deforestation on the hydrological cycle in Amazonia: a review on scale and resolution. *International Journal of Climatology* **27**(5): 633.

Dickinson R, Henderson-Sellers A. 1988. Modeling tropical deforestation: a study of GCM land-surface parameterizations. *Quarterly Journal of the Royal Meteorological Society* **114**(480): 439–462.

Ek M, Mitchell K, Lin Y, Rogers E, Grunmann P, Koren V, Gayno G, Tarpley J. 2003. Implementation of Noah land surface model advances in the National Centers for Environmental Prediction operational mesoscale Eta model. *Journal of Geophysical Research-Atmospheres* **108**(D22): 8851.

Emori S. 1998. The interaction of cumulus convection with soil moisture distribution: an idealized simulation. *Journal of Geophysical Research* **103**(D8): 8873–8884.

Hara M, Yoshikane T, Takahashi HG, Kimura F, Noda A, Tokioka T. 2009. Assessment of the diurnal cycle of precipitation over the Maritime continent simulated by 20-km Mesh GCM using TRMM PR data. *Journal of Meteorological Society of Japan* **87A**: 413–424.

Henderson-Sellers A, Gornitz V. 1984. Possible climatic impacts of land cover transformations, with particular emphasis on tropical deforestation. *Climatic Change* **6**(3): 231–257.

Hirose M, Nakamura K. 2005. Spatial and diurnal variation of precipitation systems over Asia observed by the TRMM Precipitation Radar. *Journal of Geophysical Research* **110**: D05106.

Hirose M, Oki R, Shimizu S, Kachi M, Higashiuwatoko T. 2008. Finescale diurnal rainfall statistics refined from eight years of {TRMM PR} data. *Journal of Applied Meteorology and Climatology* **47**(2): 544–561.

Hong S, Lim J. 2006. The WRF singlemoment 6-class microphysics scheme (WSM6). *Journal of the Korean Meteorogical Society* **42**: 129–151.

Iguchi T, Kozu T, Meneghini R, Awaka J, Okamoto K. 2000. Rain-profiling algorithm for the TRMM Precipitation Radar. *Journal of Applied Meteorology* **39**(12): 2038–2052.

Jacquemin B, Noilhan J. 1990. Sensitivity study and validation of a land surface parameterization using the HAPEX-MOBILHY data set. *Boundary Layer Meteorology* **52**(1): 93–134.

Kanae S, Oki T, Musiake K. 2001. Impact of deforestation on regional precipitation over the Indochina peninsula. *Journal of Hydrometeorology* **2**(1): 51–70.

Lean J, Warrilow D. 1989. Simulation of the regional climatic impact of Amazon deforestation. *Nature* **342**(6248): 411–413.

Lee E, Chase T, Rajagopalan B, Barry R, Biggs T, Lawrence P. 2009. Effects of irrigation and vegetation activity on early Indian summer monsoon variability. *International Journal of Climatology* **29**(4): 573–581.

Lee M, Schubert S, Suarez M, Held I, Kumar A, Bell T, Schemm J, Lau N, Ploshay J, Kim H, Yoo S. 2007. Sensitivity to horizontal resolution in the AGCM simulations of warm season diurnal cycle of precipitation over the United States and Northern Mexico. *Journal of Climate* **20**(9): 1862–1881.

Ohsawa T, Ueda H, Hayashi T, Watanabe A, Matsumoto J. 2001. Diurnal variations of convective activity and rainfall in tropical asia. *Journal of Meteorological Society of Japan* **79**: 333–352.

Ookouchi Y, Segal M, Kessler R, Pielke R. 1984. Evaluation of soil moisture effects on the generation and modification of mesoscale circulations. *Monthly Weather Review* **112**(11): 2281–2292.

Oouchi K, Noda A, Satoh M, Wang B, Xie S, Takahashi H, Yasunari T. 2009. Asian summer monsoon simulated by a global cloud-system-resolving model: diurnal to intra-seasonal variability. *Geophysical Research Letters* **36**(11): L11815.

Pan Z, Takle E, Segal M, Turner R. 1996. Influences of model parameterization schemes on the response of rainfall to soil moisture in the central United States. *Monthly Weather Review* **124**(8): 1786–1802.

Pielke R Sr 2001. Influence of the spatial distribution of vegetation and soils on the prediction of cumulus convective rainfall. *Reviews of Geophysics* **39**(2): 151–177.

Ramankutty N, Foley J. 1999. Estimating historical changes in global land cover: croplands from 1700 to 1992. *Global Biogeochemical Cycles* **13**(4): 997–1027.

Satomura T. 2000. Diurnal variation of precipitation over the Indo-China Peninsula: two-dimensional numerical simulation. *Journal of Meteorological Society of Japan* **78**: 461–475.

Segal M, Arritt R. 1992. Nonclassical mesoscale circulations caused by surface sensible heat-flux gradients. *Bulletin of the American Meteorological Society* **73**(10): 1593–1604.

Shukla J, Nobre C, Sellers P. 1990. Amazon deforestation and climate change. *Science* **247**(4948): 1322–1325.

Skamarock W, Klemp J, Dudhia J, Gill D, Barker D, Wang W, Powers J. 2005. *A Description of the Advanced Research WRF Version 2*. NCAR Tech Notes-468+ STR.

Smith T, Reynolds R. 2004. Improved extended reconstruction of SST (1854–1997). *Journal of Climate* **17**(12): 2466–2477.

Takahashi H, Fujinami T, Yasunari T, Matsumoto J. 2010. Diurnal rainfall pattern observed by TRMM-PR around the Indochina Peninsula. *Journal of Geophysical Research.* DOI:10.1029/2009 JD012155 (in press).

Takahashi H, Yoshikane T, Hara M, Yasunari T. 2009. High-resolution regional climate simulations of the long-term decrease in September rainfall over Indochina. *Atmospheric Science Letters* **10**(1): 14–18.

Takahashi HG, Yasunari T. 2006. A climatological monsoon break in rainfall over Indochina – A ingularity in the seasonal march of the Asian summer monsoon. *Journal of Climate* **19**(8): 1545–1556.

Takahashi HG, Yasunari T. 2008. Decreasing trend in rainfall over indochina during the late summer monsoon: impact of tropical cyclones. *Journal of Meteorological Society of Japan* **86**(3): 429–438. DOI:10.2151/jmsj.86.429.

Uppala S, Kallberg P, Simmons A, Andrae U, da Costa Bechtold V, Fiorino M, Gibson J, Haseler J, Hernandez A, Kelly G, Li X, Onogi K, Saarinen S, Sokka N, Allan R, Andersson E, Arpe K, Balmaseda M, Beljaars A, van de Berg L, Bidlot J, Bormann N, Caires S, Chevallier F, Dethof A, Dragosavac M, Fisher M, Fuentes M, Hagemann S, Holm E, Hoskins B, Isaksen L, Janssen P, Jenne R, McNally A, Mahfouf JF, Morcrette JJ, Rayner N, Saunders R, Simon P, Sterl A, Trenberth K, Untch A, Vasiljevic D, Viterbo P, Woollen J. 2005. The ERA-40 re-analysis. *The Quarterly Journal of the Royal Meteorological Society* **131**: 2961–3012.

Xie P, Arkin P. 1997. Global precipitation: A 17-year monthly analysis based on gauge observations, satellite estimates, and numerical model outputs. *Bulletin of the American Meteorological Society* **78**(11): 2539–2558.

